Nanoscale

Accepted Manuscript

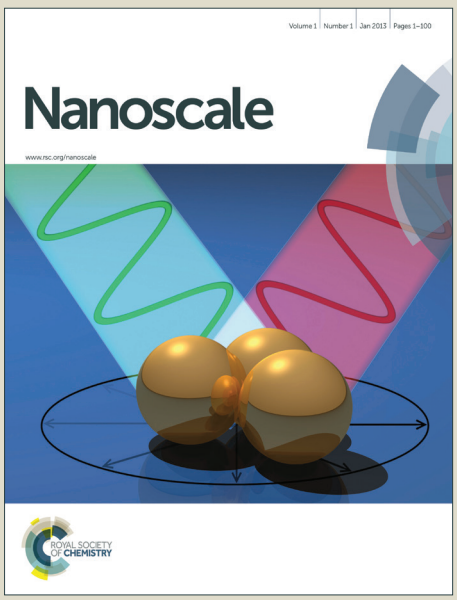

ROYAL SOCIETY OF CHEMISTRY

www.rsc.org/nanoscale

The structural transitions of C_{60} nanowhiskers under electric field characterized by *in situ* transmission electron microscopy and electron energy-loss spectroscopy

Chao Li,[a] Bingzhe Wang,[b] Yuan Yao,[a] Guangzhe Piao,[b] Lin Gu,[a] Yanguo Wang,[a] Xiaofeng Duan[a] and Richeng Yu[a,]*

In situ electrical transport measurements for individual C_{60} nanowhiskers are performed by investigation in a transmission electron microscope which monitors the crystal and electronic structure changes of the C_{60} nanowhiskers simultaneously. The electron diffraction combining with the electron energy-loss spectroscopy shows that under the external electric current, the C_{60} nanowhiskers first transform from the face-centered-cubic structure to a disordered arrangement of C_{60} molecules, then the cage structure of C_{60} molecules collapses to an amorphous carbon, finally the amorphous carbon turns to graphene stacks. This process indicates the hybridization transformation from $sp^{2.278}$ to sp^2, which is different from the transition process of C_{60} materials under high pressure. The obtained results also suggest that the stability of the C_{60} nanowhiskers should be concerned crucially when they work as electrical devices.

Key words: *C_{60} nanowhiskers, the structural transitions, in situ TEM, electric field*

1. Introduction

Since the discovery of Kroto et al., [1] C_{60} materials have attracted great interests because of their importance both in fundamental scientific researches [2] and potential technological applications such as electronic devices, [3-7] or imaging materials [8] due to their special cage structure. They usually show a hexagonal close-packed (hcp) structure in solution, while a face-centered-cubic (fcc) structure after being completely dried at room temperature. The C_{60} nanowhiskers, the single crystal with one dimensional structure composed of C_{60} molecules and a high aspect ratio (usually more than 1000) of length to diameter, can be obtained by the method of liquid-liquid interfacial precipitation (LLIP) [9,10] which makes it possible to be applied in many fields, including reservoir of materials, channels for gas or fluids, and nano-devices in both medical and electrical fields.

The electrical conductivity of C_{60} nanomaterials as field-effect transistors has already been studied. [5-7] The reported carrier mobility can reach to 11 $cm^2/V{\cdot}s$~ 2-fold higher than the highest mobility of any *n*-channel organic material (~ $6cm^2/V{\cdot}s$), [5] not to mention the solution-grown ones (1.5 $cm^2/V{\cdot}s$). Although C_{60} nanomaterials show excellent property of electrical transport, their stability as the electrical nanodevices is seldom inspected. Indeed, C_{60} nanomaterials can transform to other forms of carbon under high pressure and high temperature, such as amorphous carbon (sp^2-rich or sp^3-rich), polycrystalline diamond, microcrystalline graphite. [11-20] Under high pressure, the C_{60} nanomaterials with cage structure can transform into sp^2-rich [11,12] or sp^3-rich [13-18] carbon, depending on the condition of compression (non-hydrostatical or hydrostatical, room temperature or high temperature). Under high-temperature but atmospheric pressure, the C_{60} nanotubes and nanowhiskers can turn to graphene stacks with random orientations. [19,20] Those transformations involve the collapse of cage structure and the disorder of stacking structure, but the detail of the transition sequence has seldom been studied up to date. Wang et al. claimed that under high pressure the cages in hcp C_{60}*m-xylene are damaged first but the long-range order of the squashed clusters is still preserved with the aid of the solvent molecule at 60 GPa. [13] Hu et al. reported that the C_{60} nanotubes with fcc structure first transform to simple

cubic (sc) structure, then an isostructural phase transition occurs in the pressure range of 9.29-12.2 GPa, which is probably the result of the change in the bonding type of the C_{60} nanotubes. At last, the C_{60} nanotubes transform irreversibly to amorphous structure at 40.1 GPa. [17,18] These two results indicate that the cage structure first collapses, then the stacking structure is disarranged under pressure. However such behavior of C_{60} nanowhiskers as electrical devices under ambient pressure has not been investigated till now. In this work, *in situ* transmission electron microscopy (TEM) combining with the selected-area electron diffraction (SAED) and electron energy-loss spectroscopy (EELS) was applied to research into the stability of C_{60} nanowhiskers under the electric current. The SAED patterns provide the information on the long-range order structure, while the plasmon loss spectrum of EELS displays the feature of the electronic state and chemical bonding. [16] The combination of these techniques profiles the phase change of the C_{60} nanowhiskers directly and reveals a transformation path significantly different from the process under high pressure.

2. Experiments

The C_{60} nanowhiskers used in this work were fabricated by LLIP. The pristine C_{60} powder (MTP Ltd. 99.5%) was dissolved in pyridine, and then the pyridine solution of C_{60} was added into isopropyl alcohol in a proper mixture ratio. One minute ultrasonic dispersion was taken to obtain suitable diffusion at the interface. [21-24] In order to promote the growth of the C_{60} nanowhiskers, the solution was exposed to the visible light, such as blue light with a central wavelength of 468 nm. [22,23] The structure of the C_{60} nanowhiskers was characterized by TEM (FEI Tecnai F20). To carry out *in situ* electrical measurements in TEM, the C_{60} nanowhiskers were picked up by a gold wire electrode which is loaded to the Nanofactory *in situ* holder (ST 1000), and were controlled by a piezo-manipulator. An individual C_{60} nanowhisker was selected to attach to the other gold tip electrode. While performing the electrical measurements, the illumination electron beam in TEM was blocked to acquire the intrinsic behavior.

3. Results and discussion

Fig. 1 (a) is a morphology of a C_{60} nanowhisker with the diameter about 200 nanometers. The high resolution

TEM (HRTEM) and SAED images (Fig. 1b) show that the pristine nanowhisker is crystalline with fcc structure ($Fm\bar{3}m$, a= 1.424 nm) [21] and the growth direction is along $[0\,\bar{1}1]$. It is found that the fibers with diameters larger than 300 nm usually have hollow structure (C_{60} nanotubes) whereas those with diameters smaller than 200 nm do not show the hollow structure (C_{60} nanowhisker). [25] Using electron holography, we can easily distinguish the C_{60} nanowhiskers and nanotubes. [26] The resistance of C_{60} nanowhisker measured by *in situ* TEM electrical probing system is about 10 MΩ, which is two orders of magnitude higher than the resistance obtained by four probe method. [18] This implies that there is a large contact resistance between the gold tip and the C_{60} nanowhisker.

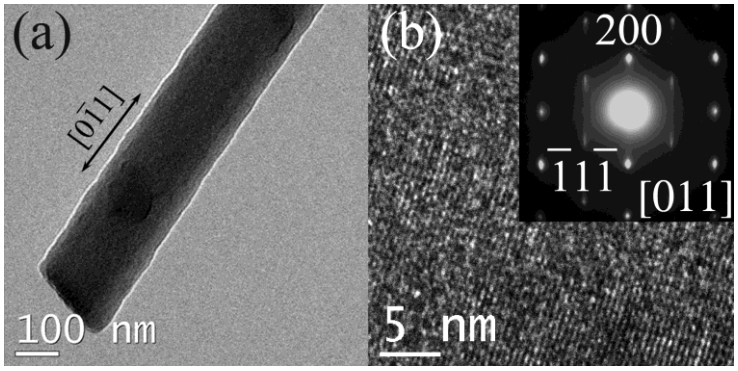

Fig. 1 Microstructure of C_{60} nanowhisker: (a) a low magnification morphology image of the C_{60} nanowhisker, which grows along the $[0\,\bar{1}1]$ direction, (b) the HRTEM image of the C_{60} nanowhisker, the inset is the SAED pattern of C_{60} nanowhisker, these images show that the starting material is crystalline.

The first interesting morphology variation under external bias is the size change of the C_{60} nanowhisker. Fig. 2 demonstrates the change of diameter of the C_{60} nanowhisker under different bias. It is apparent that the diameter of the C_{60} nanowhisker shrinks significantly at the initial stage of applying bias but expands slightly when the applied voltage increases to 3 V, while the whisker structure is still maintained. Considering the large contact resistance and low current, the observed size change may be driven by the Joule heat from the contact interface. It is hard to determine the accurate temperatures at the C_{60} nanowhisker, so the applied electric power is used here to represent the heating effect, as shown

in Fig. 3.

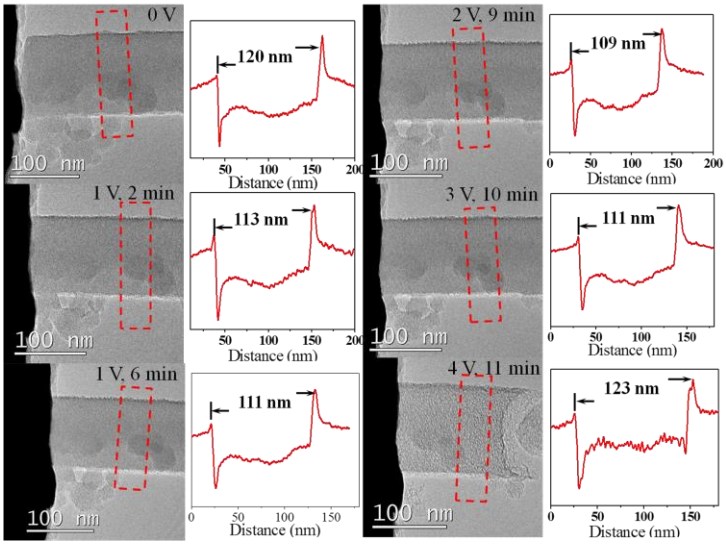

Fig. 2 The changes of morphology during the different electric fields applied on the C_{60} nanowhisker.

Fig. 3(a) displays the diameter variation with the corresponding input power of the *in situ* TEM holder, indicating qualitatively the relationship between the morphology variation and the heat effect. Although the real power applied to the nanowhisker itself should be less than the input power, the tendency of the size change could be interpreted explicitly. The SAED patterns and HRTEM images (Fig. 3(b) and (c)) of the C_{60} nanowhisker were obtained at the same time, which are employed to trace the structure transformation process. The original C_{60} nanowhisker exhibits a sharp electron diffraction pattern in SAED as same as Fig. 1(b), this fact indicates the good crystalline C_{60} at the beginning. When 1 V is applied to the nanowhisker, the diffraction pattern becomes blurred rings in 2 minutes (insert in Fig. 3(b)) and the corresponding HRTEM image (Fig. 3(b)) shows an amorphous structure. Keeping 1 V bias, the current through the nanowhisker increases from 20 nA to about 1.3 μA in 8 minutes, which implies a drop of the electric resistance of the C_{60} nanowhisker or a better electrodes contact due to the Joule heating. For 4 V, the current jumps dramatically to near 10.4 μA and the diffraction pattern (insert in Fig. 3(c)) depicts the sharp rings of graphene-based materials with extended domains. The crystallographic structure is however turbostratic instead of

graphitic as shown by the occurrence of limited number of rings. Correspondingly, the HRTEM image (Fig. 3(c)) shows the randomly orientated layers with the spacing of 0.35 nm. The sharp rise of the current may be a reasonable result of the transformation from the semiconductor C_{60} crystal to the conductor graphene-based materials. By contrast, more than half an hour irradiating of 200 kV electron beam in TEM cannot evoke the breakdown of long range order in the diffraction patterns (not shown here). Thus not the high energy electron beam but the current heating triggers the phase change of the C_{60} nanowhisker.

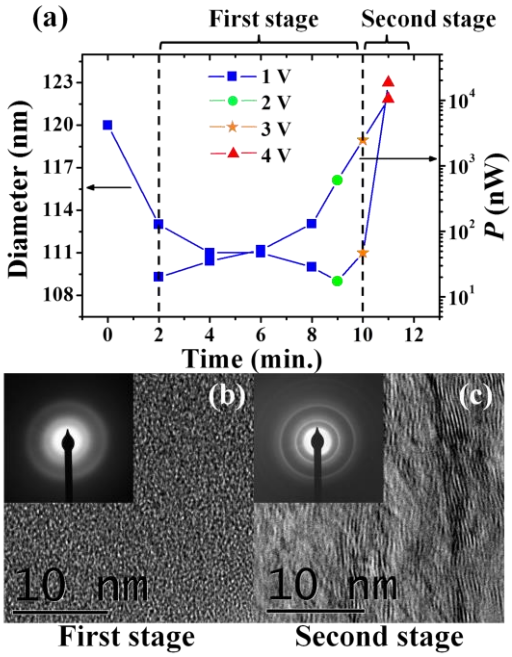

Fig. 3 (a) The changes of diameter and of power of the electric field with time. (b) and (c) The SAED and HRTEM patterns of the material obtained synchronously when the electric field is applied to the nanowhisker.

However, due to the molecule crystal nature of the C_{60} solid with cages as the stack units, both cage collapse and cage disorder can lead to the "amorphous" status showing the diffusion rings in diffraction (Fig. 3(b)). So SAED could not tell what happens during the amorphization. To clarify the path of the structure change, we acquire EELS of the nanowhisker under different voltages since it can provide the information on the electronic state and chemical bonding status which reflect the configuration of the carbon atoms. The EELS spectra were acquired in diffraction mode. The

collection semiangle is about 0.64 mrad. The characteristic semiangle θ_E is about 20/2*200000 =0.05 mrad, so the main contribution for the EELS spectra comes from the electron whose transformation of momentum is $q_\perp$. The plasmon-loss spectra of EELS acquired under different voltages are shown in Fig. 4, with criterions from amorphous carbon, C_{60} films [27] (The EELS spectrum was acquired in transmission with a 170 KeV spectrometer and the main contribution for the EELS spectrum comes from the electron whose transformation of momentum is $q_{//}$), five layers of graphene [28] (The EELS spectrum was acquired in a scanning transmission electron microscope (STEM) with the angles conditions favoring to observe the surface and bulk plasmons excited with q parallel to a.) and graphite [29] for comparison. The second peak positions of amorphous carbon (~25 eV), five layers of graphene (~18 eV) and graphite (~26.5 eV) are labelled in Fig. 4. Two bulk plasmon peaks at approximately 6 and 24.5 eV are observed in the EELS of primitive C_{60} nanowhisker. The first peak (π-plasmon) is attributed to the π-π^* interband transitions and the second peak ($\pi+\sigma$ plasmon) is related to the oscillation of whole π and σ electrons. [30] It should be mentioned that the first peak of primitive C_{60} nanowhisker is much weaker than that of C_{60} films. [27, 30] The intensity of the π-plasmon of the primitive C_{60} nanowhisker is much higher than that of the amorphous if we just compare the two spectra. Since we put all the spectra together in one figure, the difference between amorphous carbon and the primitive C_{60} nanowhisker is not so significantly presented. The intensity of π-plasmon for C_{60} cages is almost unchanged at two minutes under 1 V though the corresponding diffraction spots disappear in Fig. 3(b), which reveals that C_{60} cages are still maintained at the initial heating stage but the fcc long range order has been damaged. The intensity of π-plasmon becomes as weak as the amorphous carbon, implying that the cage structure may collapse gradually. Moreover, higher voltages push the $\pi+\sigma$-plasmon to the lower energy position of graphene stacks, [28, 31-34] opposite to the reported $\pi+\sigma$ peak of the graphite, [29] with a significant rise of the intensity of π-plasmon at 6 eV. The peak shift in the EELS demonstrates that the crystalline carbon in the nanowhisker under higher current may be an intermediate status between the multi-layer graphene and the crystal graphite. [28, 29, 31, 33] The relative increase of π-plasmon proportion also indicates the transition

from $sp^{2.278}$ hybridization[2] in the C_{60} nanowhisker to sp^2 hybridization in graphene stacks. By contrast, the experiment of C_{60} nanowhiskers under different time scale at a fixed electric field is carried out. It is found that the diameter of a C_{60} nanowhisker decreases and the current increases as time increases when the electric field was fixed at 1V and the C_{60} nanowhisker with fcc structure transfers to amorphous carbon. However, the phase transformation from amorphous carbon to graphene stacks was not observed when the electric field was fixed.

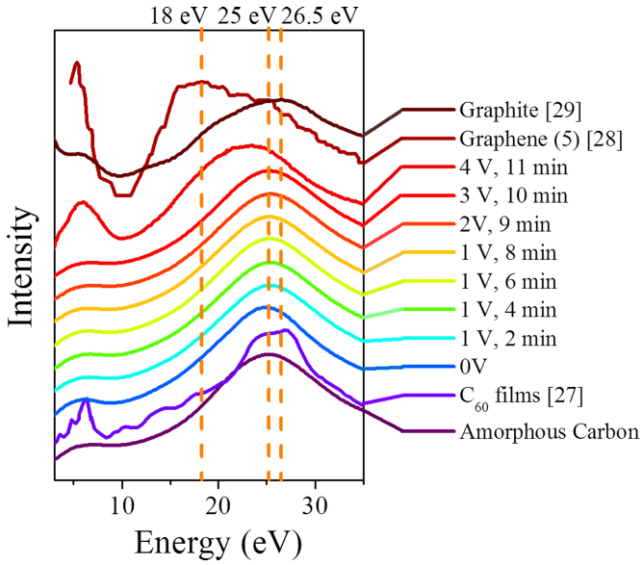

Fig. 4 The EELS in a low-loss region of the transformational process from C_{60} crystalline nanowhisker to graphene stacks.

The transformation process is summarized in Fig. 5. The C_{60} nanowhisker with fcc structure first becomes disordered arrangement of C_{60} molecules. Then the cages of C_{60} molecules collapse and change into amorphous carbon. Finally, the amorphous carbon becomes graphene stacks with random orientation not only on the radial direction but also on the axial direction of the nanowhisker under the electric heating. This process is different from those results under high pressure. As mentioned above, under high pressure, at first the cage structure collapses, then the stacking structure becomes disordered. [13,17,18] Generally, the C_{60} crystals transform to diamond or amorphous carbon with sp^3 hybridization under high pressure [13-18] or to graphite with sp^2 hybridization under high temperature, [19,20] though

following the phase diagram of carbon, [11] we can see that there are some exceptions that the C_{60} transforms to graphite under high pressure and high temperature. [11,12] In our work, the driving force for transformation should be the Joule heating in the high vacuum environment, similar to the previous reports in which the C_{60} nanotubes and nanowhiskers turn to graphene stacks with random orientations at 3000 °C. [19,20] Indeed, the gold tip was found to be melted at the point touching the C_{60} nanowhisker during *in situ* characterization sometimes, certifying that the local temperature is very high. The discrepancy between our result and the high pressure results may come from the different effects of pressure and temperature on the C_{60} nanomaterials. As is well known, both high temperature and high pressure can cause the transformation. Under high pressure, the volume of the materials is compressed and the movement of molecules is restricted, so C_{60} cages collapse at their original positions, especially for the viscous solvent surrounded C_{60} crystal. [13,17,18] But under high temperature, without the space constraint, the fcc structure of the cages is shuffled more easily by the heating due to the weak Van der Waals interaction between C_{60} molecules. The observed result indicates that C_{60} nanowhiskers may be so fragile because of the weak interaction force that they should be protected carefully and contacted to the electrodes well if they are used as the electrical devices.

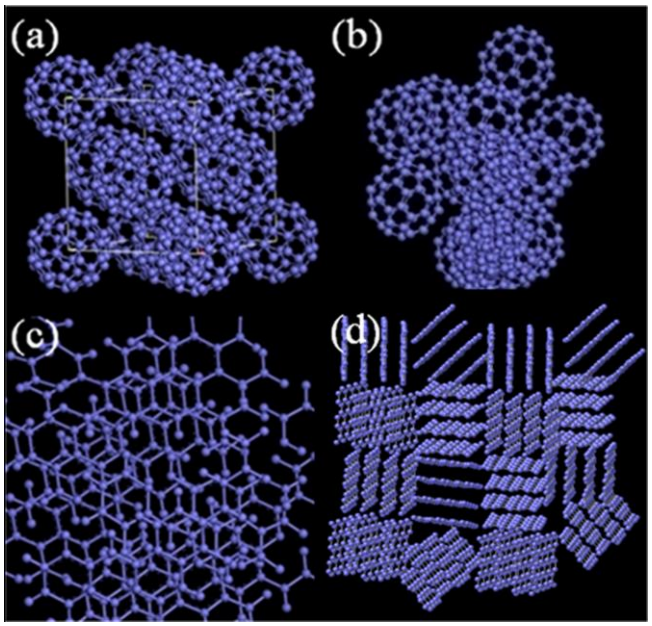

Fig. 5 The schematic diagram of the material structures during the transformational process: (a) the C_{60} nanowhiskers with fcc structure, (b) the C_{60} molecules with disordered arrangement, (c) the cage structure of C_{60} molecule collapses and the amorphous carbon forms, (d) the amorphous carbon becomes graphene stacks.

4. Conclusions

The change process of the structure of C_{60} nanowhisker under external voltage has been investigated with *in situ* TEM including SAED, HRTEM and EELS. The diameter of the C_{60} nanowhisker shrinks under the current, the structure of the C_{60} nanowhisker transforms from fcc order to the layered graphene stacks, through the intermediate amorphous status, driven by the Joule heating. The EELS reveals that the long range order of the fcc structure is broken prior to the collapse of the C_{60} cage due to the fragile bonding of the molecular crystal and then the carbon fragments from the degraded C_{60} form the layered sp^2 carbon stacks, which is different from the phase change in the high pressure studies. This structure variation under a very low voltage indicates that the C_{60} nanowhisker may be sensitive to the Joule heating and its stability should be considered seriously when it is assembled to the electronic device.

Acknowledgements

This work was supported by the State Key Development Program for Basic Research of China (Grant Nos. 2012CB932302 and 2010CB934202), the National Natural Science Foundation of China (Grant Nos. 10974235 and 11174336) and the Program for International S&T Cooperation Projects in the Ministry of Science and Technology of China (2011DFA50430).

Notes and References

[a]*Beijing National Laboratory for Condensed Matter Physics, Institute of Physics, Chinese Academy of Sciences, P. O. Box 603, Beijing 100190, P. R. China.*

[b]*Key Laboratory of Rubber-plastics, Ministry of Education, School of Polymer Science and Engineering, Qingdao University of Science and Technology, Qingdao 266042, P. R. China.*

**Corresponding Author: Tel: +86 10 82649159. E-mail address: rcyu@aphy.iphy.ac.cn (R. C. Yu).*

1 W. Kroto, J. R. Heath, S. C. O'Brien, R. F. Curl and R. E. Smalley, *Nature*, 1985, **318**, 162-163.

2 T. L. Makarova, *Semiconductors*, 2001, **35**(3), 243-278.

3 C. Dekker, *Phys. Today* 1999, **52**, 22-28.

4 K. Ogawa, T. Kato, A. Ikegami, H. Tsuji, N. Aoki, Y. Ochiai, J. P. Bird, *Appl. Phys. Lett.*, 2006, **88**, 112109.

5 H. Y. Li, B. C. K. Tee, J. J. Cha, Y. Cui, J. W. Chung, S. Y. Lee, Z. N. Bao, *J. Am. Chem. Soc*., 2012, **134**(5): 2760-2765.

6 A. Nigam, G. Schwabegger, M. Ulla, R. Ahmed, II Fishchuk, A. Kadashchuk, C. Simbrunner, H. Sitter, M. Premaratne, V. R. Rao, *Appl. Phys. Lett.* 2012, **101**, 083305.

7 Y. J. Xing, G. Y. Jing, J. Xu, D. P. Yu, H. B. Liu, Y. L. Li, *Appl. Phys. Lett.*, 2005, **87**, 263117.

8 M. Mikawa, H. Kato, M. Okumura, M. Narazaki, Y. Kanazawa, N. Miwa, H. Shinohara, *Bioconjugate Chem.*, 2001, **12**(4), 510-514.

9 K. Miyazawa, A. Obayashi, M. Kuwabara, *J. Am. Ceram. Soc*., 2001, **84**(12), 3037-3039.

10 K. Miyazawa, Y. Kuwasaki, A. Obayashi, M. Kuwabara, *J. Mater. Res.*, 2002, **17**(1), 83-88.

11 C. S. Yoo, W. J. Nellis, *Science*, 1991, **254**, 1489-1491.

12 J. L. Hodeau, J. M. Tonnerre, B. B. Favre, M. N. Regueiro, J. J. Capponi, M. Perroux, *Phys. Rev. B*, 1994, **50**, 10311-10314.

13 L. Wang, B. B. Liu, H. Li, W. G. Yang, Y. Ding, S. V. Sinogeikin, Y. Meng, Z. X. Liu, X. C. Zeng, W. L. Mao, *Science*, 2012, **337**, 825-828.

14 D. D. Liu, M. G. Yao, Q. J. Li, W. Cui, L. Wang, Z. P. Li, B. Liu, H. Lv, B. Zou, T. Cui, B. B. Liu, B. Sundqvist, *J. Raman Spectrosc*., 2012, **43**, 737-40.

15 M. N. Regueiro, P. Monceau, J. L. Hodeau, *Nature*, 1992, **355**, 237-239.

16 H. Hirai, K. I. Kondo, *Phys. Rev. B*, 1995, **51**(21), 15555-15558.

17 J. Y. Hu, S. C. Liang, G. Z. Piao, S. J. Zhang, Q. H. Zhang, Y. Yang, Q. Zhao, K. Zhu, Y. L. Liu, L. Y. Tang, Y. C. Li, J. Liu, C. Q. Jin, R. C. Yu, *J. Appl. Phys.*, 2011, **110**, 014301.

18 J. Y. Hu, N. N. Niu, G. Z. Piao, Y. Yang, Q. Zhao, Y. Yao, C. Z. Gu, C. Q. Jin, R. C. Yu, *Carbon*, 2012, **50**, 5458-5462.

19 R. Kato, K. Miyazawa, T. Nishimura, Z. M. Wang, *J. Phys.: Conf. Ser.*, 2009, **159**(1), 012024.

20 K. Asaka, R. Kato, Y. Maezono, R. Yoshizaki, K. Miyazawa, T. Kizuka, *Appl. Phys. Lett.*, 2006, **88**, 051914.

21 K. Miyazawa, J. Minato, T. Yoshii, M. Fujino, T. Suga, *J. Mater. Res.*, 2005, **20**(3): 688-695.

22 G. B. Li, P. Liu, Z. Han, G. Z. Piao, J. Zhao, S. X. Li, G. Y. Liu, *Mater. Lett.*, 2010, **64**(3), 483-485.

23 Y. T. Qu, S. C. Liang, K. Zou, S. X. Li, L. M. Liu, J. Zhao, G. Z. Piao, *Mater. Lett.*, 2011, **65**(3): 562-564.

24 J. Minato, K. Miyazawa, T. Suga, *Sci. Technol. Adv. Mater.*, 2005, **6**, 272-277.

25 J. Minato, K. Miyazawa, *Diamond Relat. Mater.*, 2006, **15**, 1151–1154.

26 Y. Yang, N. N. Niu, C. Li, Y. Yao, G. Z. Piao, R. C. Yu, *Nanoscale*, 2012, **4**, 7460-7463.

27 E. Sohmen, J. Fink, W. Krätschmer, *Z. Phys. B-Condensed Matter*, 1992, **86**, 87-92.

28 T. Eberlein, U. Bangert, R. R. Nair, R. Jones, M. Gass, A. L. Bleloch, K. S. Novoselov, A. Geim, P. R. Briddon, *Phys. Rev. B*, 2008, **77**, 233406.

29 C. Karthik, J. Kane, D. P. Butt, W. E. Windes, R. Ubic, *J. Nucl. Mater.*, 2011, **412**, 321-326.

30 R. Kuzuo, M. Terauchi, M. Tanaka, Y. Saito, H. Shinohara, *Jpn. J. Appl. Phys.*, 1991, **30**(10B), L1817-1818.

31 O. Stephan, D. Taverna, M. Kociak, K. Suenaga, L. Henrard, C. Colliex, *Phys. Rev. B*, 2002, **66**, 155422.

32 J. P. Reed, B. Uchoa, Y. II Joe, Y. Gan, D. Casa, E. Fradkin, P. Abbamonte, *Science*, 2010, **330**, 805-808.

33 J. Lu, K. P. Loh, H. Huang, W. Chen, A. T. S. Wee, *Phys. Rev. B*, 2009, **80**, 113410.

34 C. Kramberger, R. Hambach, C. Giorgetti, M. H. Rümmeli, M. Knupfer, J. Fink, B. Buchner, L. Reining, E. Einarsson, S. Maruyama, F. Sottile, K. Hannewald, V. Olevano, A. G. Marinopoulos, T. Pichler, *Phys. Rev. Lett.*, 2008, **100**, 196803.